Proceedings of ASME Turbo Expo 2011
GT2011
June 6-10, 2011, Vancouver, British Columbia, Canada

GT2011-46308

A Numerical and Experimental Investigation of the Effects of Flow Ratio on the Flow and Performance Characteristics of a Twin Entry Radial Turbine

M. R. Shahhosseini
School of Mechanical Engineering
I. Azad University
Tehran, Iran

A.Hajilouy-Benisi
Associate Professor, School of Mechanical Engineering,
Sharif University of Technology
Tehran, Iran

M. Rajabian
School of Mechanical Engineering
I. Azad University
Tehran, Iran

ABSTRACT

In this paper, a numerical and experimental investigation of the performance and internal flow field characteristics of the twin-entry radial inflow turbine under full and partial admission conditions are presented. The turbine is tested on a turbocharger test facility which was developed for small and medium size turbochargers. The flow pattern in the volute and impeller of a twin-entry turbine is analyzed using a fully three-dimensional viscous program. The computational performance results are compared with the experimental results, and good agreement is found. The flow field at the outlet of the turbine is investigated using a five-hole pressure probe. Numerical and experimental results are obtained for both full and partial admission conditions. In the volute, results show that the highest entropy gain factor belongs to the tongue. In the inlet of the rotor, a large variation in the incidence angle is displayed at the extreme conditions, leading to large incidence losses. Entropy distribution contours at the rotor exit plane are evaluated. For full admission, the location of low entropy gain at this plane occupies a region near the shroud and near the hub pressure surface corner which corresponded to a region of high absolute flow angle. Results show that the entropy gain factor patterns do not have appreciable differences at full and partial admission conditions when more flow is located at the volute shroud side. However, in the extreme cases low entropy gain at the shroud side occupies a relatively large region, and this region is increased when shroud side volute is fully closed.

INTRODUCTION

Turbochargers are widely used in the automotive engines. A radial inflow turbine is a common choice for turbochargers for small and medium size engines where exhaust energy is utilized. Multi-cylinder engines with divided exhaust manifolds lead to multiple entry turbines for pulsating turbocharging. In these applications, the turbine has usually a twin-entry. This turbine is usually exposed to partial admission conditions in engine operating conditions, where the flows in each inlet are not equal most of the time. This partial admission varies from zero flow in one entry with full admission in the other, to full flow in both entries [1]. A better understanding of this kind of turbine flow field at various operation conditions permits a better matching of the turbine to the engine. Dale and Watson [2] obtained performance of the twin-entry turbine over a wide range of partial admission conditions experimentally. They showed that at partial admission, the turbine efficiency is highest when more flow is in the shroud side entry than that of the hub side entry. They also showed that the efficiency at the extreme conditions is always lower than at full admission. No explanation for this phenomenon was put forward. Copabianco and Gambarotta [3] evaluated the performance characteristics of full and partial admission conditions for different twin-entry turbines. They showed mass flow parameter and efficiency were always higher for the hub side entry fully closed than for the shroud side entry fully closed at the extreme cases. This trend is also seen in the results of Yeo and Baines [4].

A number of researchers investigated the flow field of single and twin-entry turbines both experimentally and theoretically. The flow through the turbine is complex, compressible, viscous and three-dimensional. There are many experimental flow field investigations for a single entry volute [4-10]. Benisek [11] carried out measurements upstream and downstream of a single entry turbine rotor. The results showed that at 0.05 mm above the rotor the flow is more prone to pass from the shroud side. Twin-entry turbine flow field investigation under partial

 Copyright © 2011 by ASME

admission conditions is rare in open literature. Lymberoppoulos et al [12] published experimental and numerical study on the flow field in a twin-entry volute under partial admission conditions. The computational model was based on a quasi three-dimensional solution of the Euler equation. Baines and Yeo [13] performed experimental volute flow field investigation using laser-two-focus velocimeter under full and partial admission conditions. Hajilouy and Baines [14] acquired experimental data at the leading edge of the rotor under full and partial admission conditions using a laser-two-focus velocimeter. Zangeneh et al. [15] presented a numerical three-dimensional viscous flow field in the rotor. These numerical results were compared with flow measurement results in a low speed radial inflow turbine. These rotor exit plane results showed that the highest loss occurs at the shroud near the suction side of the rotor. Kitson [16] developed a Dawes Navier-Stokes solver to predict the flow field in the rotor. This showed that, in the exit region of the rotor a large positive swirl exists near the shroud suction surface corner. Laser- Doppler velocimeter measurements were carried out in the turbine rotor by Kreuz- lhli et al [17]. They carried out Laser-Doppler velocimeter measurements in the turbine rotor, and a numerical flow field evaluation at the rotor inlet was performed. The results of single entry turbine testing showed that the axial component of velocity decreases with distance from the hub and that the highest circumferential velocity is detected near the suction surface. Murugan et al [18] performed LDV measurements at the rotor exit. These results revealed a complex flow pattern near the tip region at the rotor exit.

Little investigation has been performed relative to understanding rotor flow behavior in radial turbine at partial admission conditions, particularly at extreme cases. An experimental study of flow fields at the rotor inlet and exit planes under partial admission conditions was performed by Yeo and Baines [19]. Various experimental methods were used to measure flow field in the turbine. Flow measurements at rotor inlet and exit region of turbomachinery were made with pneumatic probes in Refs [20-22]. Benisek [23] compared laser and five-hole probes flow measurement results at the turbocharger turbine rotor inlet and exit. The results showed acceptable agreement between these two-measurement methods especially in the rotor inlet.

The purpose of this paper is to investigate the performance and flow field characteristics of the twin-entry radial inflow turbine under full and partial admission conditions with a special focus on partial admission conditions where more flow passes through the shroud side entry and the extremes of partial admission conditions where one entry is fully closed and where highest and lowest efficiencies are obtained. The mechanisms causing different turbine performance characteristics under full and partial admission conditions are investigated. A three-dimensional computational model representing the complete turbine stage (volute and rotor) is developed. This numerical model is validated against results and exit plane flow field measurements, acquired with a five-hole pressure probe. Following this, a description of the turbine performance characteristics and flow structures within the volute and turbine passages, at full and partial admission conditions are presented. Entropy distribution contours at the exit plane for these operating conditions is evaluated.

NOMENCLATURE

$\dot{m}$	Mass flow rate
σ	Entropy gain factor
R	Gas constant, Radius
y^+	Nondimensional wall distance
φ	Azimuth angle
S	Entropy
U	Rotational speed
C_s	Isentropic expansion velocity
b	width
x	Distance from hub

Subscripts and Superscripts

h	Hub side
s	Shroud side
tip	Rotor leading edge

EXPERIMENTAL FACILITY

The turbocharger test rig has been designed, established and equipped to investigate different automotive turbochargers under a variety of operational conditions based on simulation of a turbocharger by compressed air. The main specifications of the test, which was carried out in the rig, are as follows:

1) A steady flow test using a compressor to absorb and measure the power of the turbine.

2) Full and partial admission measurements on a twin-entry turbine using a twin-inlet test system. The arrangement of the test rig facility is shown schematically in Fig. 1.

Three screw compressors are employed to produce high-pressure air adjustable up to 13 bar gauge with a mass flow rate of 0.4 kg per sec. The main compressed air supply line is a 3 inch diameter pipe. The mass flow rate is adjusted using a electro-pneumatic valve. In order to measure the steady mass flow rate, three turbine side and one compressor side orifice, plates, calibrated to BS 1042 are used [19]. The compressed air can be heated up to 200 degrees Celsius using an electrical heater unit. This prevents the condensation of any water vapor at the turbine blades, where there is a high temperature drop due to the air expansion. The heater unit consists of 32 elements, each 2 kW power, suitable for various mass flow rates and different temperature rise conditions. A turbocharger compressor absorbs the turbine output power, and acts as a dynamometer, to control the rotational speed of the turbocharger. The compressor outlet air passes through an additional throttle valve and is exhausted to the atmosphere out of the lab by a two inch exit duct. In addition, the mass flow rates to the twin-entry can be controlled independently. Full admission condition to the turbine occurs when the control valves of each entry are fully opened. Partial admission flow

Copyright © 2011 by ASME

condition is achieved by varying the flow in each entry. An error analysis and uncertainties of flow measurement system are discussed in Ref [20].

Using the schematic shown in Fig.2, the performance characteristics of a twin-entry radial inflow turbocharger turbine are investigated in this test rig under full and partial admission conditions The geometrical details for this turbine are presented in Table.1.

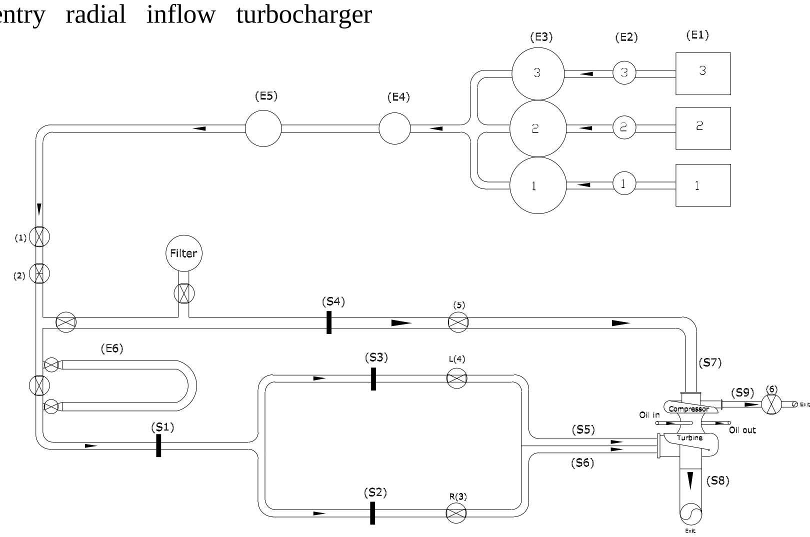

E1: Screw compressors
E2: Water traps
E3: Storage tanks
E4: Micro trap
E5: Micro filter
E6: Electrical heater
T: Turbocharger turbine
C: Turbocharger compressor
1-6: Electro- Pneumatic valves

S1: Station 1, main line mass flow rate measurement
S2: Station 2, outer limb mass flow rate measurement
S3: Station 3, inner limb mass flow rate measurement
S4: Station 4, compressor inlet mass flow rate measurement
S5: Station 5, inner limb temp. & press. measurement
S6: Station 6, outer limb temp. & press. measurement
S7:Station 7, compressor inlet temp. & press. measurement
S8:Station 8, turbine exit temp. & press. measurement
S9:Station 9, compressor exit temp. & press. Measurement

Figure 1. Turbocharger test rig

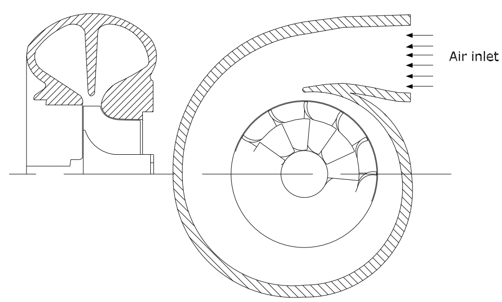

Figure 2. Schematic of the twin-entry radial inflow turbine

Table 1. Turbine geometry

Geometric feature	Radial turbine
Volute inlet area (m^2)	0.0022
Rotor inlet mean diameter (m)	0.0736
Rotor inlet blade height (m)	0.0088

Copyright © 2011 by ASME

Exducer hub diameter (m)	0.0233
Exducer shroud diameter (m)	0.0576
Number of blades	11

THE FIVE- HOLE PROBE

The detailed flow surveys of the turbine are obtained at the rotor exit by traversing a five-hole probe to obtain measurements in a plane 3.4 cm downstream of the rotor exducer trailing edge, as shown in Fig.3. The five-hole probe head configuration used for experimented testing is shown in Fig.4. The probe is approximately 25 cm in length with a stem diameter of 3 mm at the tip. The probe was installed at a fixed position in combination with the non-nulling technique. The probe is capable of measuring the flow properties such as total and static pressure as well as flow velocity and angle without requiring it to be moved or rotated during the tests.

The probe calibration is performed by inserting the probe into a specially designed calibration rig that has accurate means of measuring the flow properties according to Refs [26-28]. The calibration rig provides a steady uniform flow field of known properties at fixed direction. For calibration, the probe is rotated on the traversing mechanism; the rotation of the probe permits us to measure the pressure distribution at the tip for a previously defined set of angle combinations (pitch and yaw). This combination covers the range of incidence angles that are expected during the actual tests. At each orientation the readings of the five manometers, P_i(i=1,2,3,4,5), are recorded. The yaw, pitch and velocity coefficients are defined as:

$$\text{Yaw coefficient} = \frac{P_{p3} - P_{p2}}{P_{p1} - \frac{1}{4}(P_{p2} + P_{p3} + P_{p4} + P_{p5})} \quad (1)$$

$$\text{Pitch coefficient} = \frac{P_{p5} - P_{p4}}{P_{p1} - \frac{1}{4}(P_{p2} + P_{p3} + P_{p4} + P_{p5})} \quad (2)$$

$$\text{Velocity coefficient} = \frac{P_{pt} - P_{ps}}{P_{p1} - \frac{1}{4}(P_{p2} + P_{p3} + P_{p4} + P_{p5})} \quad (3)$$

P_{pt} and P_{ps} are the total and static pressure of the measured flow. P_{ps} is determined from the averaging of pressure 2 to 5 and P_{pt} is determined from the calibration test results [22].

The calibration curves and the relations between yaw, pitch coefficients versus yaw, and pitch angles and velocity coefficient versus yaw and pitch angles are determined. Therefore, when the probe is inserted into an unknown flow, P_1 to P_5 are obtained and the coefficients are calculated. Using the calibration curves and these values, the actual yaw and pitch angles, as well as flow velocity are found.

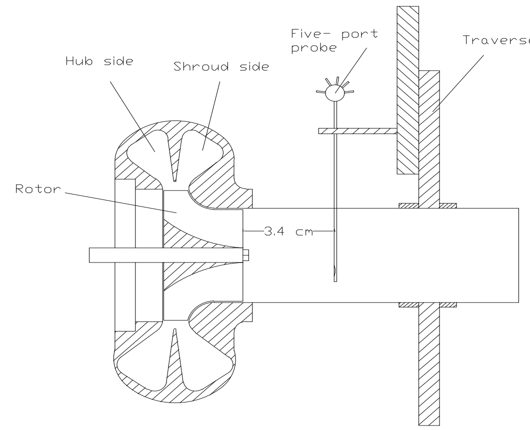

Figure 3. Schematic of five-hole pressure probe location

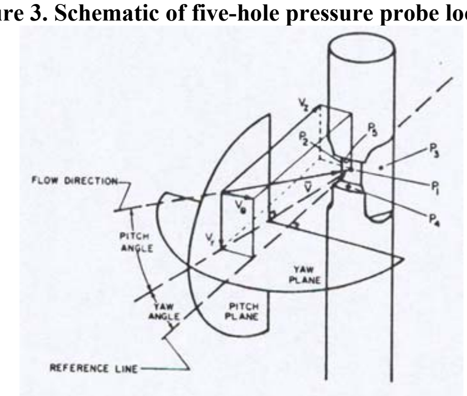

Figure 4. Five-hole pressure probe head arrangement[22]

NUMERICAL TECHNIQUE

The flow pattern in the volute and impeller of a twin-entry turbine is analyzed using a fully three-dimensional viscous program. Using a finite volume method, the Favre-averaged Navier-Stokes equations (FANS), which describes the conservation of mass, momentum and energy is used. The Favre-averaging procedure leads to a useful form of governing equations for compressible flows, and results in equations very similar to the Reynolds-averaged incompressible case. Averaged equations are then discretized by evaluating them at the center of each side known as the integration point. The Reynolds stress term in the momentum transport equations is resolved using the (RNG) k-e turbulence model [17 and 29]. For the determination of the near-wall velocities, the logarithmic wall function is used with y^+ value of 30, which is recommended in Refs [15 and 30]. For interface consideration the whole passage is solved simultaneously with circumferential “averaging” between rotating and stationary regions. As shown in Fig. 5A, the computational domain consists of the volute, rotor, and the turbine rotor downstream

Copyright © 2011 by ASME

passage extending one axial chord downstream from the trailing edge. The twin-entry inlet pipe passage is extended to 3D, which provides fully developed flow. The unstructured tetrahedral grid is applied to the entire turbine domain. The overall mesh elements used in the computational domain was 1,269,134 cells. In near wall regions tip leakage and boundary layer effects are modeled using the 3D prism elements shown in Fig. 5B.

At solid boundaries, i.e., volute, blades, hub, and shroud surfaces, no slip and no heat transfer, adiabatic wall, conditions are imposed. In the computational domain, the boundary conditions at the inlet and exit are derived from the experimental measurements. At the inlet boundary, total pressure and temperature are used. At the outlet boundary, mass flow rate is employed. For this analysis, the flow is assumed to reach a steady state solution when the normalized residuals of velocities reach 10^{-3} [30], and pressure reach 10^{-5}.

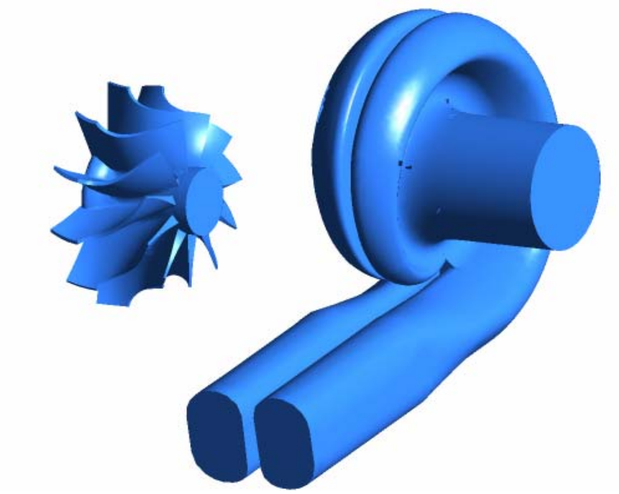

A. Turbine rotor and complete assembly model

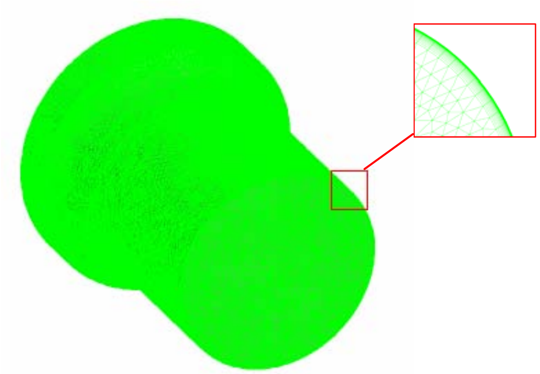

B. Turbine rotor mesh

Figure 5. Computational domain, (A) Turbine rotor and complete assembly model, and (B) Turbine rotor mesh

COMPARISON TO EXPERIMENT

Predicted total-to-static isentropic efficiency is compared with the experimental results, for a range of pressure ratios at 30000 rpm at full admission conditions. As shown in Fig. 6, reasonable agreement is obtained with a maximum difference of 3%. A noticeable discrepancy is observed at the lower pressure ratios. Fig. 7 shows the comparison of predicted and measured flow angles. It is clear that in all cases the predicted values are in good agreement with the experimental values. The largest discrepancy is observed at the shroud side which may be due to over tip leakage.

.

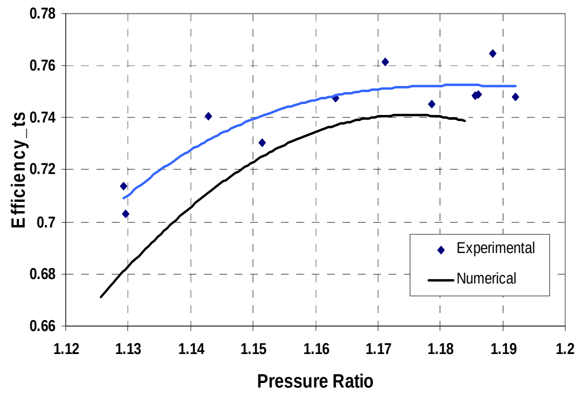

Figure 6. Predicted and experimental results of the turbine efficiency

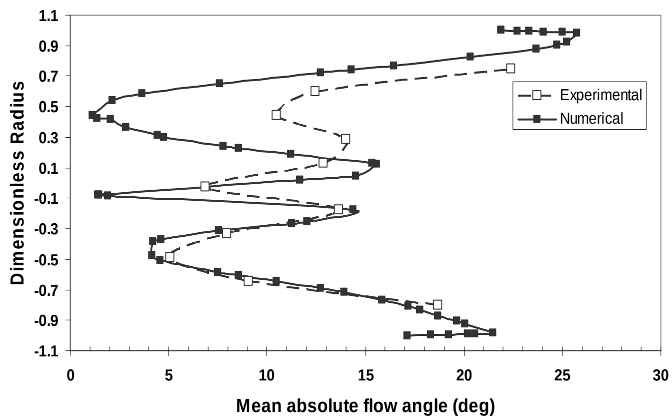

Figure 7. Predicted and experimental results of the turbine rotor exit absolute flow angle

RESULTS AND DISCUSSION

The steady state performance of the twin-entry radial turbine was investigated at 30000 rpm. Fig.8, illustrates the measured isentropic total-to-static efficiencies versus speed ratio for the full and partial admission conditions when the mass flow of the shroud side entry is higher than the hub side, $\dot{m}_s/\dot{m}_h = 1.15$. Fig.8 also illustrates the measured isentropic total to static efficiencies from the extremes of partial admission conditions when the whole flow is in one entry. It can be observed from Fig.8 that the highest efficiency corresponds to the partial admission condition at $\dot{m}_s/\dot{m}_h = 1.15$ and lowest efficiency is for the extreme case where the hub shroud side entry is fully closed. In order to understand the mechanism of losses and the fluid dynamic processes in a twin-entry turbine at different conditions, the flow field was analyzed for the entire turbine.

Copyright © 2011 by ASME

This analysis was carried out at a velocity ratio 0.7 for the full admission condition and 0.71 for the partial admission condition $\dot{m}_s/\dot{m}_h = 1.15$ where the peak efficiency generally occurs. In the extreme partial admission conditions the pressure ratio and mass flow rates for the shroud side entry, $\dot{m}_s/\dot{m}_h = \inf$, were the same as for the hub side entry, $\dot{m}_s/\dot{m}_h = 0$. The total mass flow rate in all cases was almost equal.

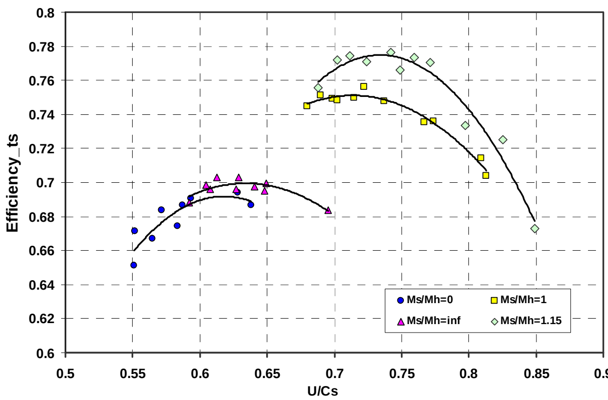

Figure 8. Experimental results of the turbine efficiency under full and partial admission conditions for 30000 rpm

VOLUTE FLOW FIELD

The velocity contours in the turbine volute at the radial-tangential plane are presented in Fig. 9 for x/b equal to 0.2 and 0.8. As shown in Figs. 9A and 9B, the variation of velocity demonstrates some distortion near the tongue of volute with only a slight velocity variation detected at x/b=0.2 and 0.8. In addition, these profiles show periodic fluctuations near the rotor due to the effect of the passing turbine rotor blades. It is also observed, that the influence of rotor does not extend very far upstream, and only a slight dependence on x/b is observed. Figs. 9C and 9D show that the lowest entropy gain factor is near the volute tongue, where entropy gain factor is defined as $\sigma = e^{(\frac{-S}{R})}$. An entropy gain factor equal to one corresponds to the highest quality, and lower than one represents poorer quality. Fig. 10 shows cross-flow velocity vectors in the volute for an azimuth angle of 180 deg, at full and partial admission conditions. Fig.10A shows that the cross velocity is predominantly in a radial inward direction. This velocity component becomes highest at the outlet of volute. Fig. 10B, shows the effect of the divider where the radial inward component of velocity decreases. This causes the losses to increase due to the mixing and interaction between the two streams. The low momentum flow is predicted to exist just downstream of the divider. Fig. 10C shows that radial velocity pattern does not have an appreciable difference at full and partial admission conditions when more flow is in the shroud side of the volute. Figs. 10D and 10E show cross-flow velocity vectors at partial admission conditions when the whole flow is in the hub side entry or the shroud side entry. It can be seen, that reversed flow exists in the entry with the lower inlet total pressure. In addition, the velocity decreases from the wall to the center of volute which suggests a strong force vortex at this section of the volute. The mixing of the two streams occurs just downstream of the divider, and is deflected towards the lower inlet total pressure side. Figs. 10D and 10E illustrate that at $\dot{m}_s/\dot{m}_h = 0$ there is a strong flow migration from the hub side towards the shroud side at the volute exit. When $\dot{m}_s/\dot{m}_h = \inf$, the reverse effect does not occur to the same extent.

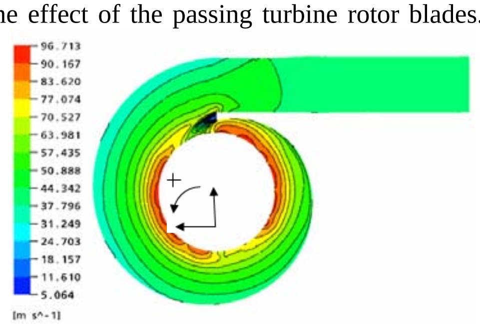

A. Absolute Velocity at x/b=0.2

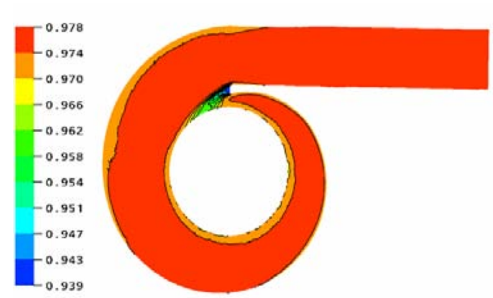

C. Entropy gain factor at x/b=0.2

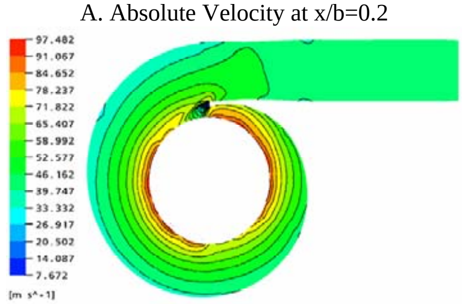

B. Absolute Velocity at x/b=0.8

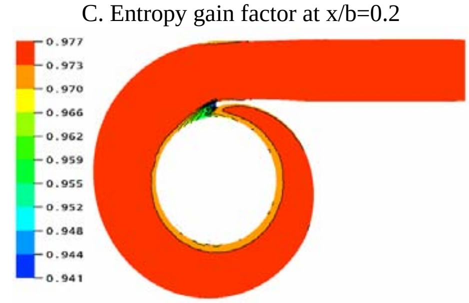

D. Entropy gain factor at x/b=0.8

Figure 9. Flow field and entropy gain factor contours in the volute sections

Copyright © 2011 by ASME

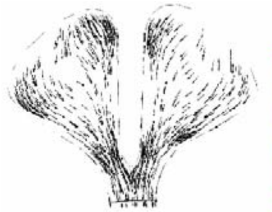

A. Full admission vector

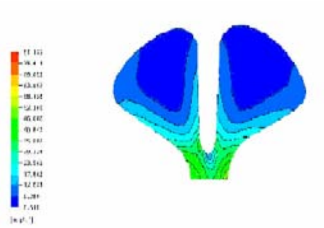

B. Full admission contour

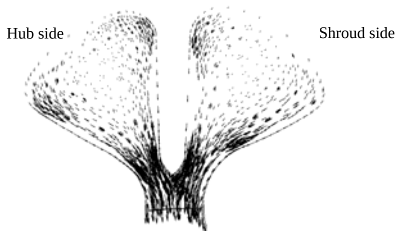

C. Radial velocity at $\dot{m}_s/\dot{m}_h = 1.15$

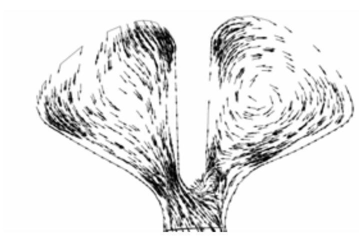

D. Radial velocity at $\dot{m}_s/\dot{m}_h = 0$

E. Radial velocity at $\dot{m}_s/\dot{m}_h = \text{inf}$

Figure 10. Variation of entropy with azimuth angle

The velocity profiles at 180 deg Azimuth angle, φ, are shown in Fig. 11 for full admission conditions and partial conditions 0.1 mm upstream of rotor. It can be seen in Figs. 11A, 11B, that as the radius ratio is reduced both the radial, and tangential components are affected. It can be seen, that the radial velocity profile becomes less uniform as the radial ratio is reduced, and this component of velocity is largest close to the wall and smallest around the center of the volute due to the boundary layer effects. Fig. 11A shows the effects of the divider located at a x/b of 0.45 to 0.55. At the divider the radial and tangential components of velocity are zero. The radial and tangential velocity components are reduced downstream of the divider at R/R_{tip}=1.08 which indicate a low momentum wake flow in this region.

Figs. 11C and 11D show the velocity profiles when hub side entry and shroud side entry is fully closed. It is noted in Fig. 11C, that the tangential velocity profiles are predominately higher on the shroud side than on the hub side. This tangential velocity component has the highest value at the R/Rtip=1.08. The radial velocity profile at this radius ratio is not uniform and is affected by the interaction of the two streams flow. It has the lowest value at the hub side, which means that these operating conditions, the flow is mostly in the shroud side. As illustrated, there is reverse flow in the hub side, because the radial velocity becomes negative at some point in the volute. Fig. 11D shows a mirror image of the tangential and radial velocity profiles. Reverse flow is also noted to occur very close to the inner wall in Fig. 11C. However, when hub side fully open at R/R_{tip}=1.08, the radial velocity is more prone to migrate continuously towards the shroud side which is not seen in the opposite case with this extension. This effect is attributed to the region of low pressure near the shroud side.

Variations of volute radial and tangential components of velocity for a fixed radius at five azimuth angles are presented in Fig. 12. It can be seen in Figs. 12A and 12B that at -15 deg, the flow is still fully guided by the passage and the velocity profile remains uniform. In addition, this profile shows a transition from a fully developed pipe flow at -15 deg to volute passage flow at the other azimuth angles. Also a comparison of the tangential component with the radial component shows that the tangential component is more uniform than the radial component as the flow moves around the volute. Figs. 12C and 12D show the velocity profiles when hub side entry and when shroud side entry are fully closed. The tangential velocity profiles remain uniform and there is some evidence of decay in the tangential velocity close to the walls in the entry with higher total pressure. It can be noted, that the highest radial velocity profile occurs closest to the divider wall. This appears to be due to the main flow being deflected towards the low-pressure entry. Fig. 12.C shows a higher negative radial velocity which suggests a strong vortex at the no flow entry. The tangential velocity profiles at $\dot{m}_s/\dot{m}_h = \text{inf}$ are mostly positive except at azimuth angle= 90 deg. The negative velocity profile at $\dot{m}_s/\dot{m}_h = 0$ occurred at azimuth angles of 90,180 and 270 deg which suggests higher loss in the no flow entry.

 Copyright © 2011 by ASME

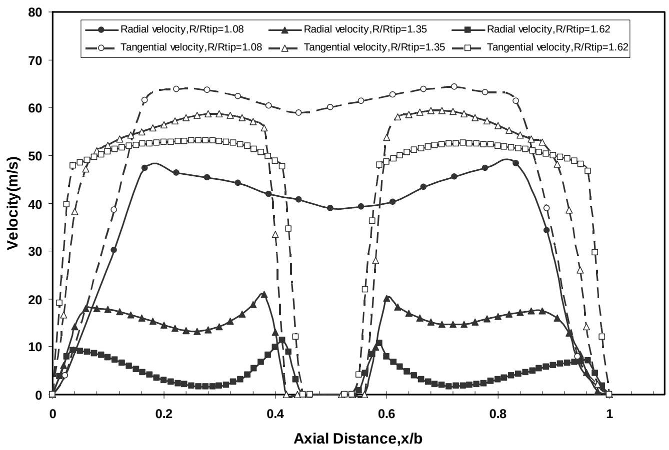

A. $\dot{m}_s/\dot{m}_h = 1$

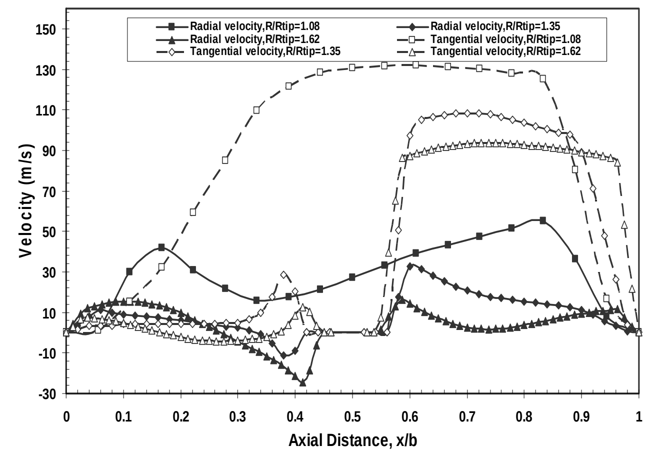

C. $\dot{m}_s/\dot{m}_h = \mathrm{inf}$

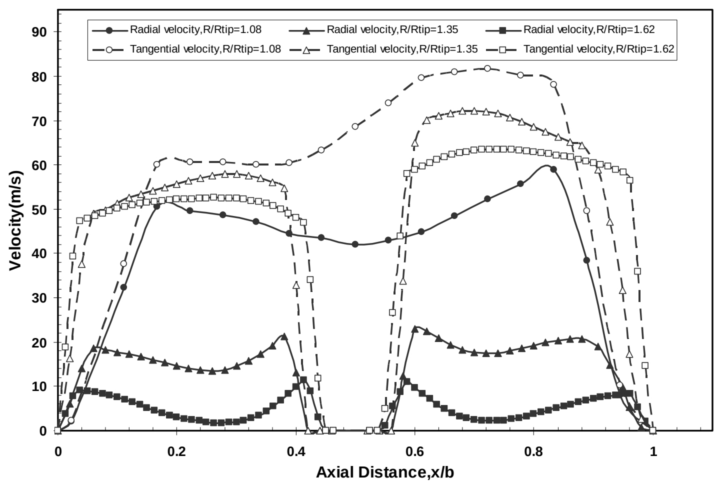

B. $\dot{m}_s/\dot{m}_h = 1.15$

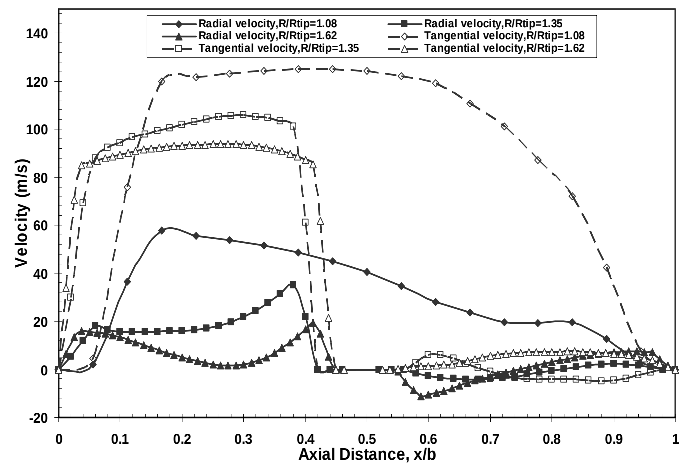

D. $\dot{m}_s/\dot{m}_h = 0$

Figure 11. Volute passage velocity profile at $\varphi = 180^o$

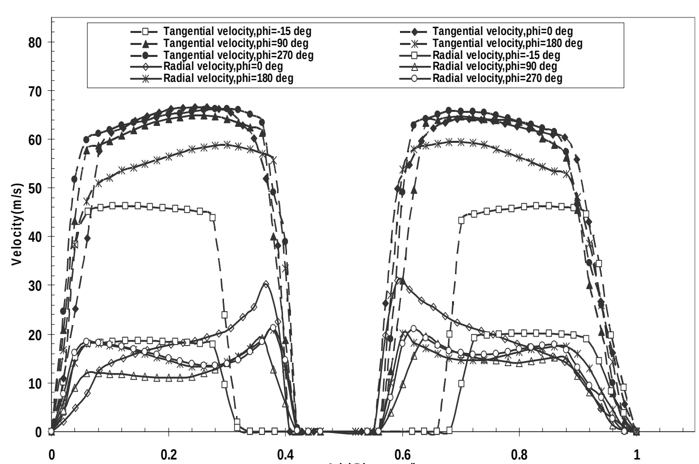

A. $\dot{m}_s/\dot{m}_h = 1$

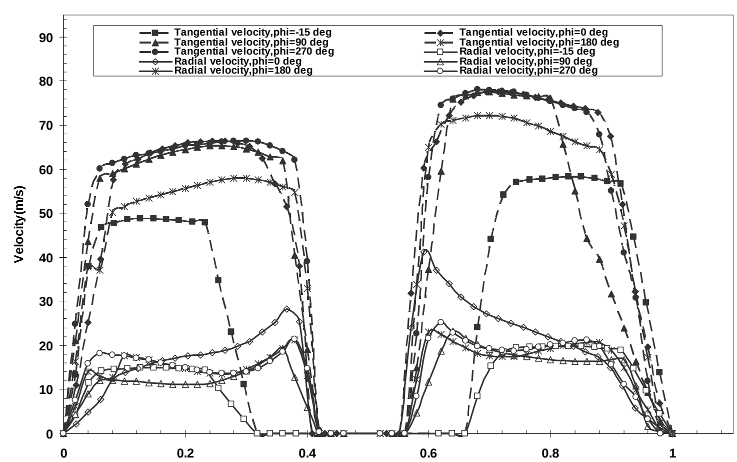

B. $\dot{m}_s/\dot{m}_h = 1.15$

Copyright © 2011 by ASME

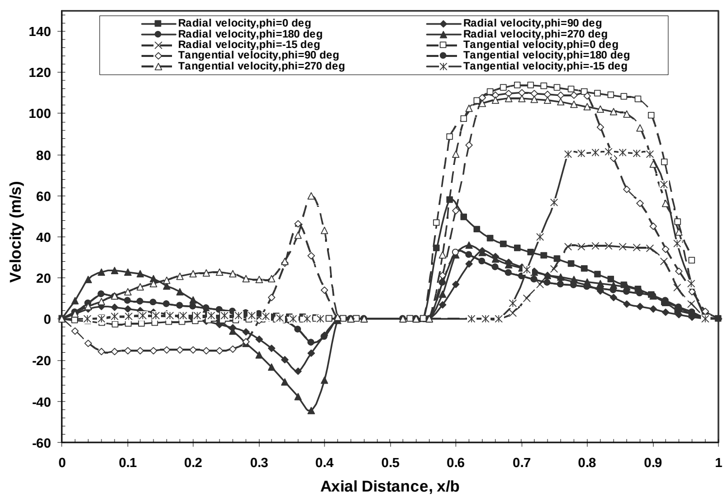

C. $\dot{m}_s/\dot{m}_h = \text{inf}$

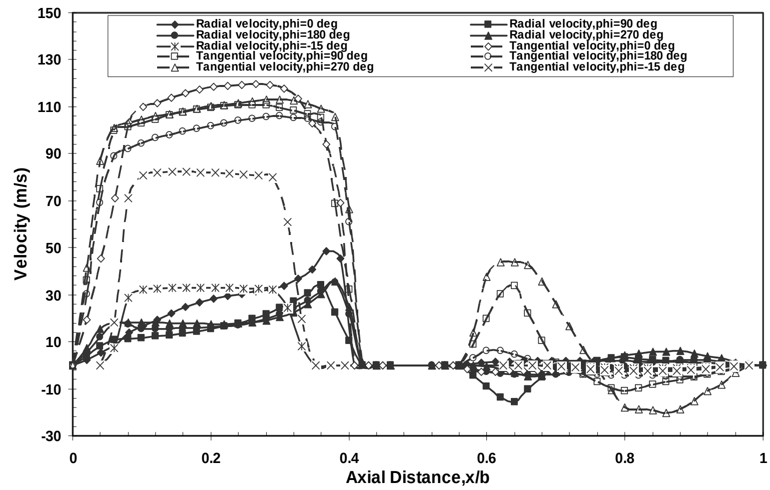

D. $\dot{m}_s/\dot{m}_h = 0$

Figure 12. Variation of radial and tangential components of velocity with azimuth angle at R/Rtip=1.35

ROTOR INLET FLOW FIELD

The velocity components and incidence angles for equal admission, and partial admission conditions at a plane 0.01 mm upstream of the rotor leading edge are presented in Fig. 13. This plane is located at 180 deg from the volute tongue, and the blade location in this figure is shown in black. As shown in Fig. 13A, the inward radial component of velocity increases from hub to shroud and a small variation can be seen from suction surface to pressure surface. It can also be observed in this figure that the flow exists the gap region between the rotor hub and the casing inner wall. The tangential component of velocity slightly increases from hub to shroud and from the pressure surface (PS) towards the suction surface (SS) which is shown in Fig.13B. The incidence angle variation is shown in Fig.13C. The optimum incidence angle varies from -20 to -40 deg, which is in agreement with Ref [31] results , and may be one of the reasons for the highest efficiency in the $\dot{m}_s/\dot{m}_h = 1.15$. The optimum incidence angle is mostly observed near the shroud side of rotor. Furthermore, this figure presents the contours of radial and tangential components of velocity and the incidence angle at partial admission conditions, $\dot{m}_s/\dot{m}_h = 1.15$, where the highest efficiency occurs. It can be seen that the radial velocity component increases from the hub to the shroud side. A large variation in tangential velocity can be noted from the pressure surface to the suction surface. This velocity component shows highest discrepancy with full admission conditions. Fig. 12F shows that the lowest incidence angle is generally near the rotor hub side.

With the hub side fully closed, Fig. 13G shows that the highest radial velocity is restricted the shroud side region. Fig. 13H shows that, the highest values of tangential velocity is spread throughout the passage. The other extreme with the shroud side fully closed shows that the highest values of radial velocity occupy all the passage, Fig. 13J. At this condition the hub side of the rotor inlet experiences a higher tangential velocity, Fig. 13K. Therefore, a greater loss is expected to generate due to mixing of high and low tangential velocities. The tangential velocity has major influence on rotor work extraction, so for the $\dot{m}_s/\dot{m}_h = 0$ condition a lower efficiency is expected due to a fact that just half of the rotor (hub side) experiences high tangential velocities.

Figs. 13I and 13L show variations of incidence angle at the inlet of the rotor for extreme conditions. With the hub side closed (Fig. 13I), the incidence angle has a mostly positive value, which is away from optimum. When the shroud side is fully closed half of the rotor experiences negative incidence angles and the other half experiences positive incidence angles. This large variation in incidence angle causes higher incidence losses and detrimental aerodynamic performance, as illustrated in Fig. 13L.

The axial component of velocity is considered by deviation angle from radial plane. Fig. 14 shows variations of deviation angle 0.01 mm before the rotor. From free vortex flow which is commonly assumed in volute design, the rotor experiences a zero spanwise component of velocity. The curvature in the meridional plane of rotor causes low pressure at the shroud side so a non-zero spanwise component of velocity upstream of rotor is expected. For full admission conditions, Fig. 14A, shows that the deviation of axial velocity component near the hub is directed towards the hub and near the shroud is directed towards the shroud side. However, in partial admission conditions when $\dot{m}_s/\dot{m}_h = 1.15$, the axial component is mostly toward the shroud side and the deviation angle is lower in this operating condition than the full admission condition. Migration of fluid toward the shroud side is stronger upstream of the turbine in this operating condition.

When the hub side fully closed, Fig. 14.C, the axial component is mostly towards the shroud side and the deviation

Copyright © 2011 by ASME

angle is reduced. However, with the shroud side fully closed, Fig. 14D, flow is a more prone to skew toward the axial direction. Therefore, migration of fluid towards the shroud side is stronger upstream of the turbine at this operating condition. A lower skewing of the flow towards the shroud side for the $\dot{m}_s/\dot{m}_h = \inf$, $\dot{m}_s/\dot{m}_h = 1.15$ and full admission conditions, and the higher skewing of flow towards the shroud side for $\dot{m}_s/\dot{m}_h = 0$ may be a good explanation for higher efficiency drop in the shroud side fully closed condition.

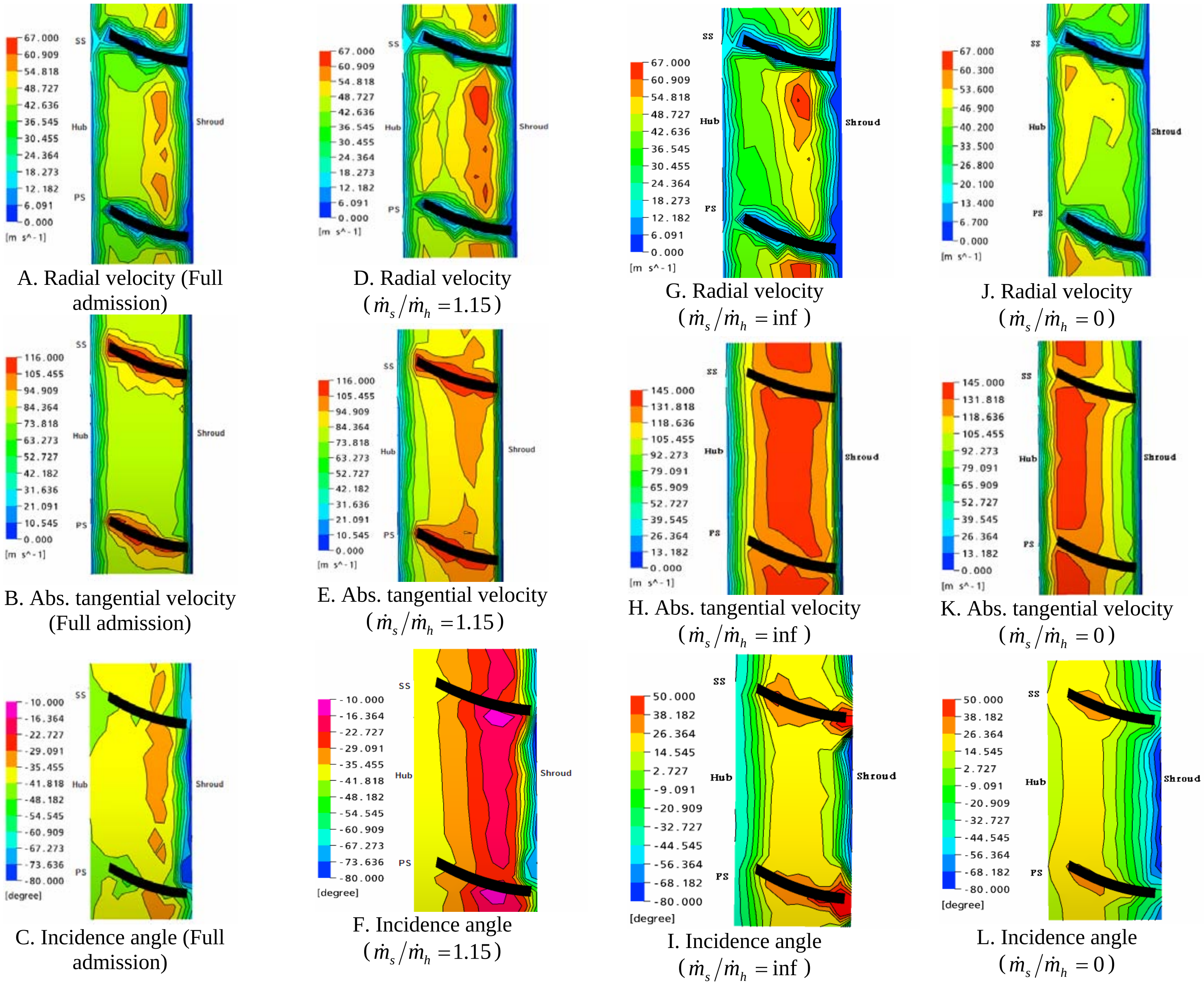

A. Radial velocity (Full admission)

D. Radial velocity ($\dot{m}_s/\dot{m}_h = 1.15$)

G. Radial velocity ($\dot{m}_s/\dot{m}_h = \inf$)

J. Radial velocity ($\dot{m}_s/\dot{m}_h = 0$)

B. Abs. tangential velocity (Full admission)

E. Abs. tangential velocity ($\dot{m}_s/\dot{m}_h = 1.15$)

H. Abs. tangential velocity ($\dot{m}_s/\dot{m}_h = \inf$)

K. Abs. tangential velocity ($\dot{m}_s/\dot{m}_h = 0$)

C. Incidence angle (Full admission)

F. Incidence angle ($\dot{m}_s/\dot{m}_h = 1.15$)

I. Incidence angle ($\dot{m}_s/\dot{m}_h = \inf$)

L. Incidence angle ($\dot{m}_s/\dot{m}_h = 0$)

Figure 13. Flow field contours at the inlet of rotor

Copyright © 2011 by ASME

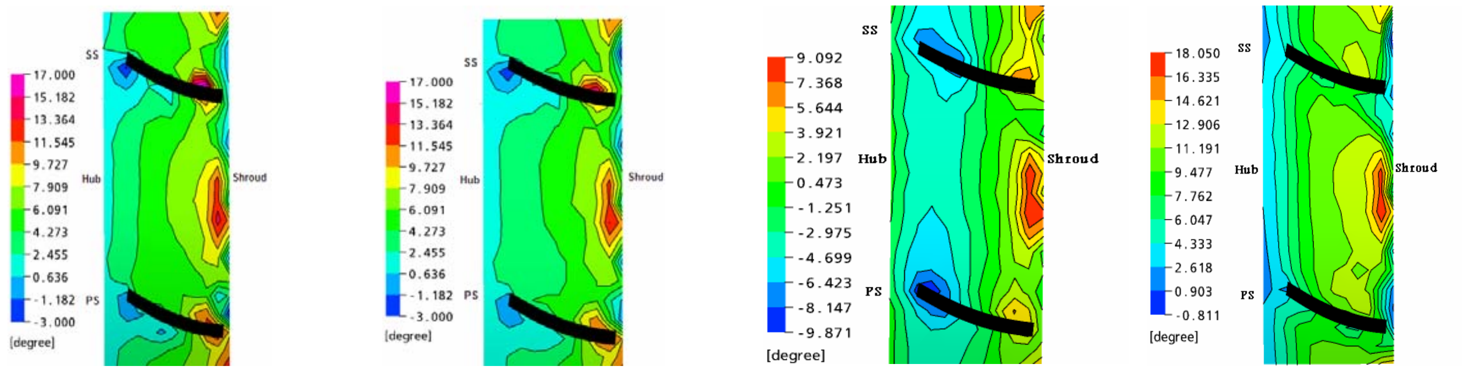

A. Deviation angle at full admission

B. Deviation angle at $\dot{m}_s/\dot{m}_h = 1.15$

C. Deviation angle at $\dot{m}_s/\dot{m}_h = \inf$

D. Deviation angle at $\dot{m}_s/\dot{m}_h = 0$

Figure 14. Flow deviation angle from radial plane at the inlet

ROTOR EXIT FLOW FIELD

In order to consider in detail the rotor exit flow field characteristics, the flow distributions at the exit plane of the turbine is presented. Fig. 15 shows the contours of the tangential component of absolute velocity under full and partial admission conditions where higher abs. tangential velocity indicates greater exit kinetic losses. As shown in this figure, the flow pattern of tangential component of velocity is generally similar at full and $\dot{m}_s/\dot{m}_h = 1.15$ conditions (Fig. 15A, Fig. 15B). In addition, Fig. 15B shows the regions of high tangential velocity at the shroud side near the suction surface and at the hub near the pressure surface, A and B, respectively. The former flow pattern can be explained by the tip clearance flow. The latter low momentum fluid region may be due to the interaction of exducer curvature effect that is moving low momentum fluid from the pressure surface towards the suction surface, and to secondary flow which tries to move low momentum fluid from the hub towards the shroud. At the extreme cases, when the whole flow is in shroud side entry, $\dot{m}_s/\dot{m}_h = \inf$, high tangential velocity in region A has a shift towards the top of mid-span, Fig. 15C. This pattern can be seen at $\dot{m}_s/\dot{m}_h = 0$,Fig. 15D. In this case, large regions are affected with high tangential velocity, which indicates extra loss generation.

The contours of exit absolute flow angle are shown in Fig. 16. This angle corresponds to the level of swirl in the flow. A large positive value of this angle indicates a condition where the flow prone to separation from suction side and negative angle indicated a condition where the flow is prone to separate from the pressure surface. It can be observed from Fig. 16. that a large positive angle is present at the shroud near the suction surface and a large negative angle is located at the hub near the pressure surface. This feature is consistent with the pattern of tangential component of abs, velocity. It is presented in Fig. 16A and 16B that this angle is reduced in partial admission conditions when more flow is in the shroud side entry than full admission conditions. It is also noted that this angle increases at $\dot{m}_s/\dot{m}_h = \inf$, Fig.16C. The highest value occurs at $\dot{m}_s/\dot{m}_h = 0$ which illustrates that the level of swirl increases at this condition, Fig. 16D.

The contours of entropy gain factor at full and partial admission are presented in Fig. 17. It is shown in Fig. 17A, that the minimum entropy gain factor accumulates at the shroud side near the suction surface and at the hub side near the pressure surface. This correlates well with the patterns of tangential velocity and flow angle, and the rest of the plane is almost loss free. Contour plots of exit plane entropy gain factor for full and partial admission conditions illustrate higher entropy gain factor at partial admission, $\dot{m}_s/\dot{m}_h = 1.15$, than comparable full admission conditions. The reason for this seems to be associated with lower flow angles and tangential component of velocity at the suction side.

Contour plots of entropy gain factor at the exit plane for extreme partial admission conditions illustrates significant entropy gain discrepancy for full admission conditions ,Figs. 17C and 17D. At these conditions, the lowest entropy gain factor is penetrated deeper toward the center of rotor and mostly occupies the upper part of the exit plane. This pattern is more pronounced for shroud side entry fully closed conditions, $\dot{m}_s/\dot{m}_h = 0$.

Copyright © 2011 by ASME

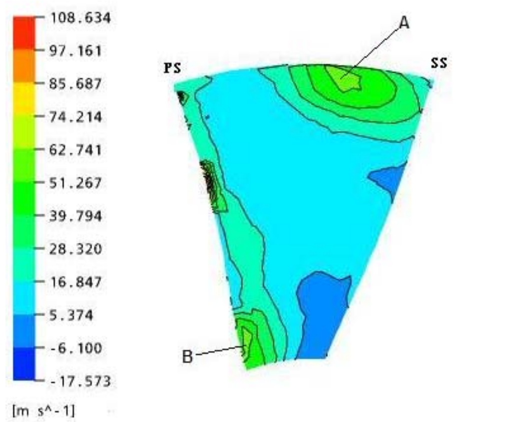

A. Relative velocity at Full admission

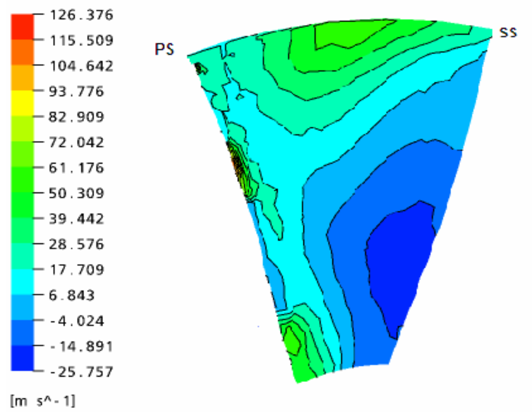

C. Relative velocity at $\dot{m}_s/\dot{m}_h = \text{inf}$

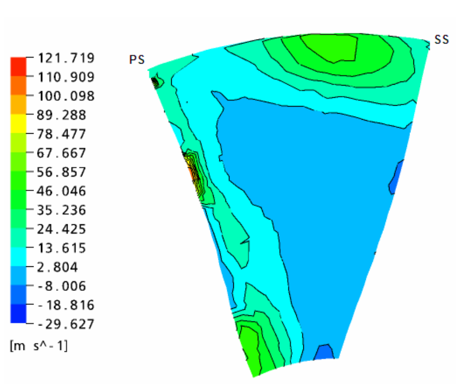

B. Absolute tangential velocity at $\dot{m}_s/\dot{m}_h = 1.15$

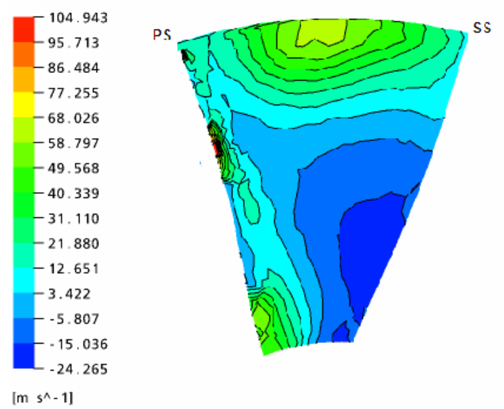

D. Relative velocity at $\dot{m}_s/\dot{m}_h = 0$

Figure 15. Velocity contours at the exit of rotor

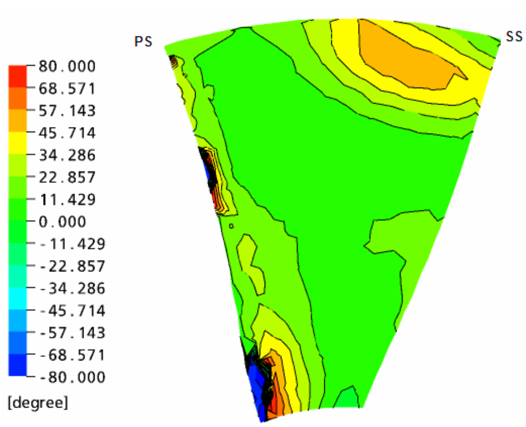

A. Absolute flow angle at Full admission

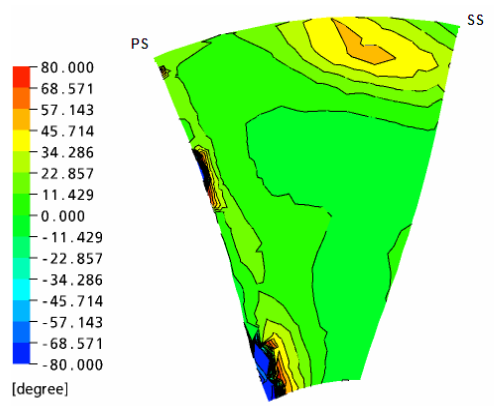

B. Absolute flow angle at $\dot{m}_s/\dot{m}_h = 1.15$

Copyright © 2011 by ASME

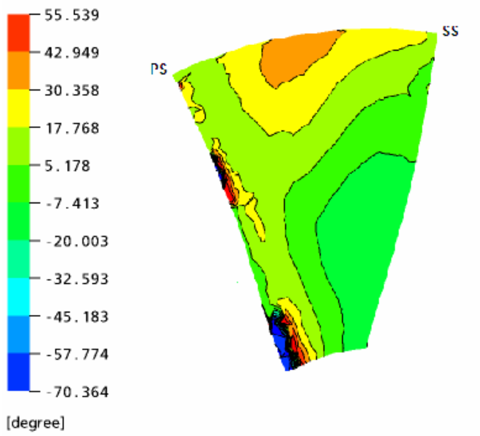

C. Absolute flow angle at $\dot{m}_s/\dot{m}_h = \text{inf}$

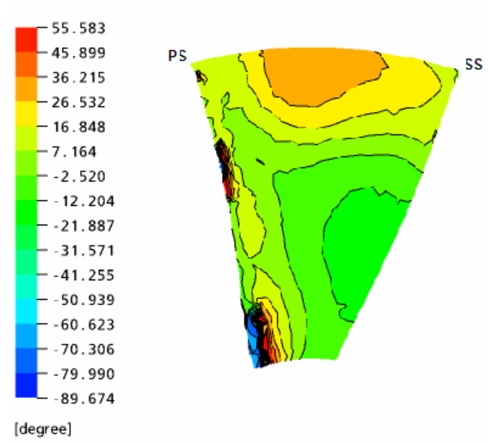

D. Absolute flow angle at $\dot{m}_s/\dot{m}_h = 0$

Figure 16. Flow angle contours at the exit of rotor

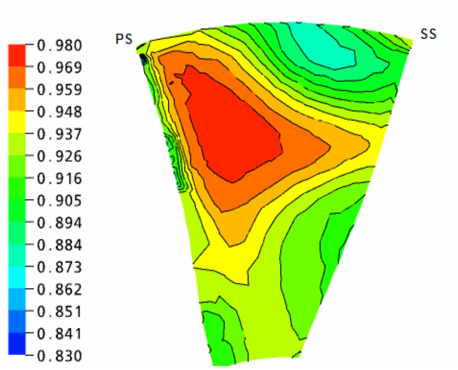

A. Entropy gain factor at Full admission

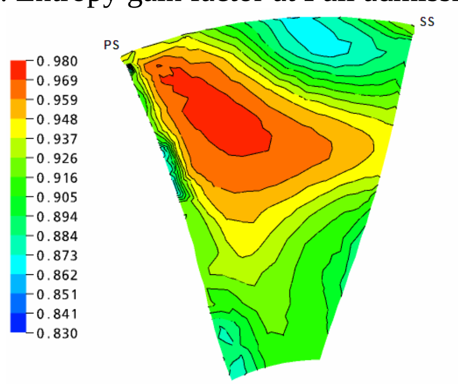

B. Entropy gain factor at $\dot{m}_s/\dot{m}_h = 1.15$

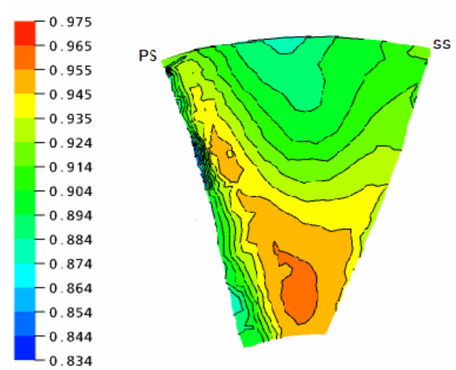

C. Entropy gain factor at $\dot{m}_s/\dot{m}_h = \text{inf}$

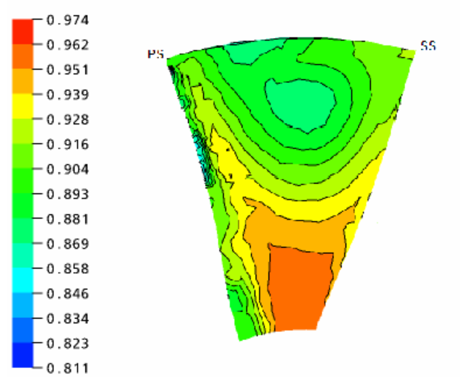

D. Entropy gain factor at $\dot{m}_s/\dot{m}_h = 0$

Figure 17. Entropy gain factor contours at the exit of rotor

CONCLUSIONS

In this paper the performance and flow field characteristics of the twin-entry radial inflow turbine are investigated under full and partial admission conditions. The experimental performance results show that efficiency characteristics are influenced by partial admission flow, and maximum efficiency occurs when more flow is present in the shroud entry at partial admission. Meanwhile, the lowest efficiency occurs when the entire flow is in hub side entry. The features of the flow field within the twin-entry turbine stage are modeled numerically under full and partial admission conditions. Good agreements in their patterns are observed between predicted and experimental performance results. In addition, absolute flow velocity and angle measurements with five-hole pressure probe were carried out downstream of the rotor. The predicted absolute angle at the turbine exit is in agreement with five-hole

Copyright © 2011 by ASME

probe measurements data. Numerical results show that the flow in the volute is three-dimensional and complex in volute tongue due to distortion near the tongue at the equal admission. The lowest entropy gain factor is obtained in this region. The radial component of velocity at the constant azimuth angle shows non-uniformity as the radius ratio is reduced. However, the tangential component shows a nearly constant flow pattern. The highest similarity to the full admission conditions is at partial admission conditions when more flow is in the shroud side. For extreme cases, velocity vectors show that at the extreme partial admission conditions, the flow circulates in the closed entry passage and higher losses are predicted. Flow field results show a complex flow pattern at both the inlet and exit of the rotor. At the inlet, a comparison of numerical results of four conditions show that the value of the tangential component of absolute velocity is higher at the hub side of the rotor at $\dot{m}_s/\dot{m}_h = 0$, and this pattern is not observed in the other cases. Meanwhile, large variations in the incidence angle within $\dot{m}_s/\dot{m}_h = 0$ indicate unfavorable conditions at the rotor inlet. In addition, the spanwise variation of flow is much greater toward shroud side and the flow direction is more prone towards the shroud side when shroud side entry is closed. Flow field modeling at the exit plane indicates that the highest swirl level is observed at the shroud side and hub side, which corresponds to lowest entropy gain factor at these two regions. The results show minimum swirl exists at $\dot{m}_s/\dot{m}_h = 1.15$. Entropy gain factor contours show entropy gain pattern do not have appreciable differences at full and partial admission conditions. At the extreme partial admission conditions the deviation of the flow angle increases. In addition, low entropy gain factor penetrate more toward the center, and this is more pronounced at $\dot{m}_s/\dot{m}_h = 0$. The turbine shows lower efficiency at the extremes of partial admission conditions when compared with full and $\dot{m}_s/\dot{m}_h = 1.15$ conditions. The lowest turbine efficiency occurs when the shroud side entry is fully closed. The reasons for this appear to be associated with the mixing of high and low fluid velocity at the inlet of the rotor, which is pronounced when the shroud side is fully closed. High positive and large variations in the incidence angle in the two extreme cases are observed. These cause greater incidence losses and result in lower efficiencies. At the extremes of partial admission conditions, the spanwise variation of flow is greater, especially in the $\dot{m}_s/\dot{m}_h = 0$, which flow is more prone to skew towards shroud side. At the exit of the rotor, results show that under extreme conditions, the flow exhibits a higher level of swirl and consequently a larger region of low entropy gain factor near the shroud, which imposes extra losses to the turbine, and causes lower work extraction from the turbine.

ACKNOWLEDGEMENTS

The authors gratefully acknowledge the support of the energy conversion center at Sharif University of Technology and the turbocharger and turbocharging laboratory staff.

REFERENCES

1. Watson N. and Janota M.S. (1982) Turbocharging the Internal Combustion Engine. Longman Scientific and Technical Publishing Company.
2. Dale, A. and Watson, N. (1986) Vaneless Radial turbocharger Turbine Performance. IMechE Conference Paper, C110/86.
3. Capobianco, M. and Gambarotta, A. (1993) Performance of a twin-entry automotive turbocharger turbine. ASME Paper 93-ICE-2.
4. Baines, N.C., and Yeo, J. H. (1991) Flow in a Radial Turbine under Equal and Partial Admission Conditions. IMechE paper C423/002.
5. Tabakoff, W., Sheoran, Y. and Kroll, K. (1980) Flow Measurements in a Turbine Scroll. Transaction of ASME, Journal of Fluid Engineering, Vol. 102, pp. 290- 296.
6. Whitfield, A. and Mohd Noor, A. B., (1990) Investigation of the Flow Characteristics of Radial Inflow Turbocharger Volutes. IMechE Conference Paper C405/023.
7. Hamed, A. and Baskharon, E. (1979) Analysis of Three Dimensional Flow in a Turbine Scroll. ASME Paper, Presented at the Winter Annual Meeting, New York City.
8. Winterbone, D. E., Nikpour, B. and Alexander, G. I. (1990) Measurement of the Performance of a Radial Inflow Turbine in Conditional Steady and Unsteady Flow. IMechE Paper C405/015.
9. Martinez-Botas, R.F., pullen, K.R., and Shi, F. (1996) Numerical calculations of a turbine volute using a 3-D Navier-Stokes Solver. ASME Paper 96-GT-66.
10. Baines, N. C. and Lavy, M. (1990) Flow in Vaned and Vaneless Stators of Radial-Inflow Turbocharger Turbines. IMechE Paper C405/005.
11. Benisek, E. F. and Struble, A. G. (1990) Laser Velocimeter Measurements in a Turbocharger Turbine. IMechE paper C405/009.
12. Lymberopoulos, N. and Baines, N. C. and Watson, N. (1988) Flow in Single and Twin Entry Turbine Volutes. ASME Paper 88-GT-59.
13. Yeo, J. H. and Baines, N. C. (1994) Laser Velocity Measurements in a Twin-Entry Vaneless Radial Turbocharger Turbine. JSME International Journal, Series B, Vol. 37, No. 4, PP. 861-870.
14. Hajilouy, A., Baines, N. (1996) Twin-Entry Radial Turbine Flow Measurements under Unsteady Flow Conditions. Fourth Annual Mechanical Eng. Conf. of ISME, pp.233-244.
15. Zangeneh-Kazemi, M., Dawes, W.N., and Howthorne, W.R. (1988) Three Dimensional Flow in Radial-Inflow Turbines. ASME Paper 88-GT-103, pp.1- 9.
16. Kitson, S. T. (1992) Aerodynamic Investigation of Radial Turbines Using Computational Methods. VonKarman Institute for Fluid Dynamics Lecture Series 1992-05.
17. Kreuz-Ihli, T. and Filsinger, D. (2000) Numerical and Experimental Study of Unsteady Flow Field and Vibration in Radial Inflow Turbines. Journal of Turbomachinery, Vol. 122, PP.247-254.

Copyright © 2011 by ASME

18. Murugan, D.M., Tabakoff, W. and Hammed, A. (1997) Flow Measurements and Flow Analysis in the Exit Region of a Radial turbine. Int. Journal of Rotating Machinery, Vol.3, pp.93-105.
19. Yeo, J. H. and Baines, N. C. (1990) Pulsating Flow Behavior in a Twin-Entry Vaneless Radial-Inflow Turbine. IMechE Paper C405/004.
20. Gilarranz, J. L., Ranz, A. J., Kopko, J. A. and Sorokes, J. M. (2005) On the Use of Five-Hole Probes in the Testing of Industrial Centrifugal Compressors. Journal of Turbomachinery, Vol. 127, pp.91-106.
21. Payne, S. J., Ainsworth, R.W., Miller, R.J., Moss, R.W. and Harvey, N.W. (2003) Unsteady Loss in a High Pressure Turbine Stage. Int. Journal of Heat and Fluid Flow, pp.698-708.
22. Miller, E. C., and L'Ecuyer, M.R. (1985) Flow Field Surveys at the Inlet and Exit of a Radial Inflow Rotor. Purdue University, Thermal Sciences and Propulsion Center, Technical report No. TSPC-TR-85-12.
23. Benisek, E.(1994)Comparisons of Laser Measurements and Pneumatic Measurements in a Turbocharger Turbine. IMechE paper C484/01/94.
24. BS-1042 (1981) Method of Measurement of Fluid Flow in Closed Conduits.
25. Rad,M., Hajilouy, A., and Shahhosseini, M. (2006) Evaluation of Empirical Performance Characteristic of Turbocharger Turbine and Compressor. 9th AIAA/ASME Joint Thermophysics and Heat Transfer Conference.
26. Morrison, G.L., Schobeiri, M.T. and Pappu, K.R. (1998) Five-Hole Pressure Probe Analysis Technique. Journal of Flow Measurement and Instrumentation, pp. 153-158.
27. Ingram, G. and Gregory-Smith, D. (2006) An Automated Instrumentation System for Flow and Loss Measurements in a Cascade. Journal of Flow Measurement and Instrumentation, pp. 23-28.
28. Dudzinski, T. J., and Krause, L.(1969) Flow Direction Measurement with Fixed-Position Probes. NASA Technical Report, TM X-1904.
29. Palfreyman. D, Martinez-Botas. R. (2005) The Pulsating Flow Field in a Mixed Flow Turbocharger Turbine: An Experimental and Computational Study. Journal of Turbomachinery, Vol. 127, pp.144-155.
30. Palfreyman. D, Martinez-Botas. R. (2002) Computational and Experimental Investigation of Aerodynamics of Turbocharger Mixed-Flow Turbines. IMechE Paper C602/017/2002.
31. Baines. N., 2002,"Radial and Mixed Flow Turbine Options for High Boost Turbochargers," IMechE Paper C602/014/2002.

Copyright © 2011 by ASME